A Meso-β-Scale Kinetic Energy Analysis of a Midlatitude Squall System

By Da-Lin Zhang and Zhiming Wang[1]

Department of Atmospheric and Oceanic Sciences, McGill University, 805 Sherbrooke Street West, Montreal, Quebec H3A 2K6, Canada
(Manuscript received 9 March 1993, in revised form 1 June 1993)

Abstract

A meso-β-scale kinetic energy (KE) budget of a midlatitude mesoscale convective system (MCS) and its effects on larger-scale flow are investigated using a 21-h high-resolution real-data simulation of an intense squall system that occurred during 10–11 June 1985 PRE-STORM. It is found that the ageostrophic cross-contour generation in the front-to-rear (FTR) ascending flow provides a major source of KE to the squall system, whereas the horizontal flux divergence is a primary sink. The vertical flux divergence is a KE sink (source) in the FTR ascending flow below (above) an upper-level jet, but it is always a source in the rear-to-front (RTF) descending flow. Due to the downward KE transport in the RTF flow, the presence of the jet stream containing most of its KE along the line appears to affect the intensity of the squall system and surface gust fronts several hundreds kilometers away to the front and to the southwest of the system.

The effects of moist convection on atmospheric motion of all resolvable scales are examined in a wavenumber space. With deep convection incorporated, the model produces little changes in the KE spectrum for smaller wavelengths but significant alterations in both the spectral magnitude and slope for longer wavelengths. The convectively generated alterations appear to be a consequence of the intermittent development of the MCS, rather than reverse KE cascade.

1. Introduction

Recent observational and modeling studies have shown that squall lines with trailing stratiform precipitation are often characterized by three distinct air currents within the systems: an overturning updraft along the leading line, a front-to-rear (FTR) ascending flow into the trailing stratiform region, and a rear-to-front (RTF) descending current beneath the stratiform cloudiness (Smull and Houze, 1987; Rutledge *et al.*, 1988; Zhang *et al.*, 1989). These internal (meso-β-scale) circulations have been found to play an important role in the formation of trailing stratiform precipitation (Rutledge and Houze, 1987; Zhang and Gao, 1989; Zhang and Cho, 1992), the interaction of mesoscale convective systems (MCSs) with larger-scale mean flow (Gao *et al.*, 1990; Gallus and Johnson, 1991), and the development of midlevel mesovortices (Biggerstaff and Houze, 1991; Zhang, 1992). These internal airflows should also have profound effects on the energetic interactions between MCSs and their environments.

However, few KE studies have been performed on the internal energetics of MCSs and their relationships with larger-scale environments, undoubtedly owing to the lack of appropriate data. For instance, on the meso-α-scale, all KE studies have been conducted with emphasis placed on MCSs' environments and the interaction between synoptic and mesoscale circulations using upper-air observations (*e.g.*, Kung and Tsui, 1975; Fuelberg and Printy, 1984; Carney and Vincent, 1986; Chen *et al.*, 1990). For these KE studies, the energetic effects of MCSs on larger-scale environments are treated only as a residual. Thus, the results could contain large errors due to the computation of other terms, particularly those associated with pressure gradients, in the KE balance equation. On the other hand, some meso-γ-scale KE budgets have been attempted to determine convective-scale energy sources and sinks, *e.g.*, using the Doppler-derived high-resolution ($\Delta x < 1$ km) winds and retrieved thermodynamic variables within MCSs (Lin and Coover, 1988; Lin *et al.*, 1991). But the lack of data in the immediate storm environments and weak-echo regions places stringent limits on the budget results. For this reason, Lilly and Jewett (1990) investigated the energetics of supercell storms using dynamically consistent data obtained

[1] Permanent affiliation: Guangdong Institute of Tropical and Oceanic Meteorology, Guangdong Province, People's Republic of China.

from cloud model simulations.

Nevertheless, all of the aforementioned mesoscale KE budgets have documented significant energy conversion and transport in the vicinity of MCSs, and considerable alteration of larger-scale energy balance. Although most of the studies reveal that generation by cross-contour flow is the main source and horizontal flux divergence is the major sink of KE, their magnitudes vary markedly, depending on the intensity and the phase of MCSs (McInnis and Kung, 1972; Kung and Tsui, 1975; Tsui and Kung, 1977). Furthermore, Vincent and Carney (1984) found pronounced differences between KE budget terms derived from the conventional and special upper-air observations, indicating that data resolution may account for a large portion of the differences in the previously-mentioned KE studies. In particular, upper-air observations in the vicinity of active MCSs are often either missing or less reliable for KE analyses. Thus, KE budget analyses of numerical simulations are valuable in aiding our understanding of the effects of MCSs.

The purposes of the present study are to (i) examine the relative importance of various internal air streams in determining the energetics of an MCS; and (ii) investigate the net energetic effects of the MCS on different scales of motion, using a 21-h, high-resolution, real-data simulation of an intense squall system that occurred during 10–11 June 1985 U.S. Preliminary Regional Experiment for STORM-Central (PRE-STORM; Cunning 1986). As compared to observations, the simulation data are much more complete and dynamically consistent. Although this dataset has been utilized by Gao *et al.* (1990) for horizontal momentum analysis, we feel that the present investigation fills the gap in the mesoscale KE studies and facilitates comparisons with the previous meso-α- and γ-scale KE analyses. In particular, because of the less terms involved the KE analysis appears to reveal better the interaction of energy-generating elements with their larger-scale environments. The presentation of this study is organized as follows. Sections 2 and 3 describe briefly the model simulation and the basic methodology used for this study, respectively. Section 4 presents vertical and horizontal distribution of meso-β-scale and area-averaged KE budgets during the squall's life cycle in order to gain insight into KE sources/sinks of the MCS. Section 5 shows the energetic effects of the squall system on its larger-scale environment, and discusses convectively generated KE spectra. A summary and concluding remarks are given in the final section.

2. Model simulation

The squall system under investigation was initiated at 2100 UTC (*i.e.*, 1500 LST) 10 June 1985 as a weak surface front moved towards the PRE-STORM network and interacted with a thermal boundary. A midlevel short-wave trough also played an important part in the initiation and later organization of the squall system. The squall line intensified rapidly in a convectively unstable environment over the network and advanced southeastward at a speed of 14–16 m s^{-1}. The squall system reached its mature stage at 0300 UTC and began to dissipate at 0600 UTC 11 June. During its mature and decaying stages, the squall system produced many classical meso-β-scale characteristics, such as a pre-squall mesolow, a mesohigh and a wake low, an overturning updraft, a FTR updraft and a RTF downdraft, a leading vortex followed by an anticyclonic vorticity zone and a midlevel mesovortex (see Johnson and Hamilton, 1988; Rutledge *et al.*, 1988; Biggerstaff and Houze, 1991).

The Pennsylvania State University/National Center for Atmospheric Research (PSU/NCAR) mesoscale model was utilized to simulate the initiation and subsequent evolution of the squall system (see Anthes *et al.*, 1987 and Zhang *et al.*, 1989 for more details). The essential model elements include: (i) a two-way interactive nested-grid procedure (Zhang *et al.*, 1986); (ii) an improved version of the Fritsch-Chappell (1980) convective scheme in which parameterized downdrafts are incorporated; (iii) explicit calculations of cloud water/ice and rainwater/snow as predictive variables (Hsie *et al.*, 1984; Zhang, 1989); and (iv) the Blackadar boundary-layer scheme (Zhang and Anthes, 1982). To simulate this squall system, the model has to be initialized with conventional observations at 1200 UTC 10 June 1985, which is 9 h prior to the initiation of the squall line. The model is then integrated for 21 h with a fine-mesh length of 25 km.

Zhang *et al.* (1989), Zhang and Gao (1989) and Zhang (1992) showed that the PSU/NCAR model reproduces remarkably well many internal structures and evolution of the squall system, as verified against all available network observations (*i.e.*, Augustine and Zipser, 1987; Johnson and Hamilton, 1988; Rutledge *et al.*, 1988; Biggerstaff and Houze, 1991). Because the 10–11 June 1985 squall line has been the subject of numerous investigations, Figs. 1 and 2 provide only a portion of the evolution of simulated surface features and vertical cross sections of total KE content, overlaid by system-relative flow vectors, from 12, 15 and 18 h simulations for convenience in later discussion. These three periods are chosen to represent roughly the squall's development at the incipient, mature and decaying stages. It is apparent that the previously mentioned surface pressure disturbances and tropospheric internal airflow structures are well reproduced in the simulation. As can be seen from height deviations, the surface pressure perturbations extend up to as high as 600 mb. Zhang and Gao (1989) showed that the

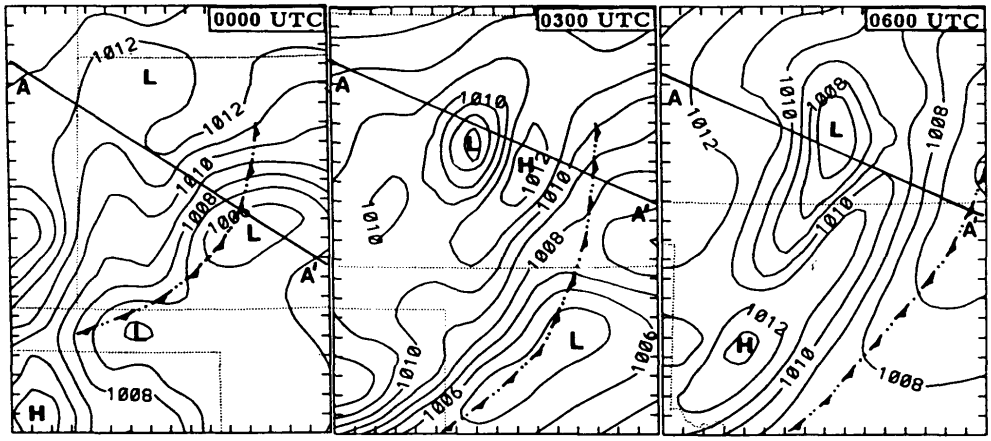

Fig. 1. Distribution of sea-level pressure (mb) from 12, 15 and 18 h simulations, valid at 0000, 0300 and 0600 UTC 11 June 1985, respectively. The cold frontal symbols alternated with double dots indicate the leading convective line. The lines with A-A′ are the location of cross sections used in the subsequent figures. The intervals marked on the frame are the fine-mesh grids (*i.e.*, 25 km), similarly for the rest of figures.

initial high KE content in the upper portion of the troposphere (Fig. 2) is associated with a southwesterly jet stream near 250 mb. As the squall line enters the mature stage (*i.e.*, 0300 UTC), a pocket of the low KE content that originated from the lower half of the troposphere becomes oriented along the FTR ascending air stream, whereas a pocket of the high KE content associated with the jet stream tends to be brought downward and forward in the RTF descending flow. Near the end of the squall's life cycle (*i.e.*, 0600 UTC), some KE content in the jet stream has reached the surface behind the system, whereas the KE content in the convectively disturbed upper troposphere has been markedly reduced. Inspection of the squall-line circulation suggests that the low-level increased and the upper-level decreased KE contents occur primarily along and normal to the line, respectively (*e.g.*, *cf.* Figs. 2 and 10 in Gao *et al.*, 1990). In addition, these KE variations appear to be closely related to the development of descending RTF and ascending FTR flows within the squall system. The next three sections show how the KE budgets are computed and how individual energetic processes contribute to the generation of these KE anomalies.

3. Methodology

A majority of previous KE budget studies have utilized an Eulerian form of equations. In the present study, a quasi-Lagrangian approach is adopted in which the budget is evaluated in coordinates following the squall system, in order to separate the system's advective effects from the energetic processes that influence the KE changes. The KE equation for a hydrostatic atmosphere (see Fuelberg and Printy, 1984) in the quasi-Lagrangian p-coordinates can be approximated as

$$\underset{\text{TEN}}{\frac{DK}{Dt}} = \underset{\text{HFD}}{-\int \nabla\cdot[(\boldsymbol{V}-C\boldsymbol{n})]k} \underset{\text{VFD}}{-\int \frac{\partial \omega k}{\partial p}} \underset{\text{GEN}}{-\int \boldsymbol{V}\cdot\nabla\phi} + \underset{\text{DIS}}{\int \boldsymbol{V}\cdot\boldsymbol{F}}, \tag{1}$$

where

$$\int = \frac{1}{g\Delta x\Delta y\Delta p}\int dxdydp, \tag{2}$$

and

$$\frac{D}{Dt} = \frac{\partial}{\partial t} + C\frac{\partial}{\partial n}, \tag{3}$$

$C\boldsymbol{n}$ is the system propagation speed normal to the line, $k=\boldsymbol{V}\cdot\boldsymbol{V}/2=(u^2+v^2)/2$ is the horizontal KE per unit mass and $K=\int k$, $\phi=gz$ is the geopotential height, ω is the vertical velocity in the p-coordinates, $\Delta x=\Delta y=25$ km is the grid length, $\Delta p=50$ mb, and $\boldsymbol{F}$ denotes the frictional effects associated with numerical diffusion and the planetary boundary layer (PBL). The terms HFD and VFD are horizontal and vertical flux divergence of KE, respectively. They have no effects on the total KE of MCSs over a large area, but can redistribute KE within the MCSs and transfer it from one scale to another. Note that to compute the HFD term, the model (x, y) components of winds (*i.e.*, u and v) have been transformed into the right-handed coordinates (n, s) with n-axis normal to the line, positive in its direction of movement (*i.e.*, V_n and V_s). The system propagation speed is then subtracted from its normal component (*i.e.*, an average speed of 14.5 m s^{-1} along the direction of 125^0). Thus, the HFD term should be viewed as being relative to the squall system. The

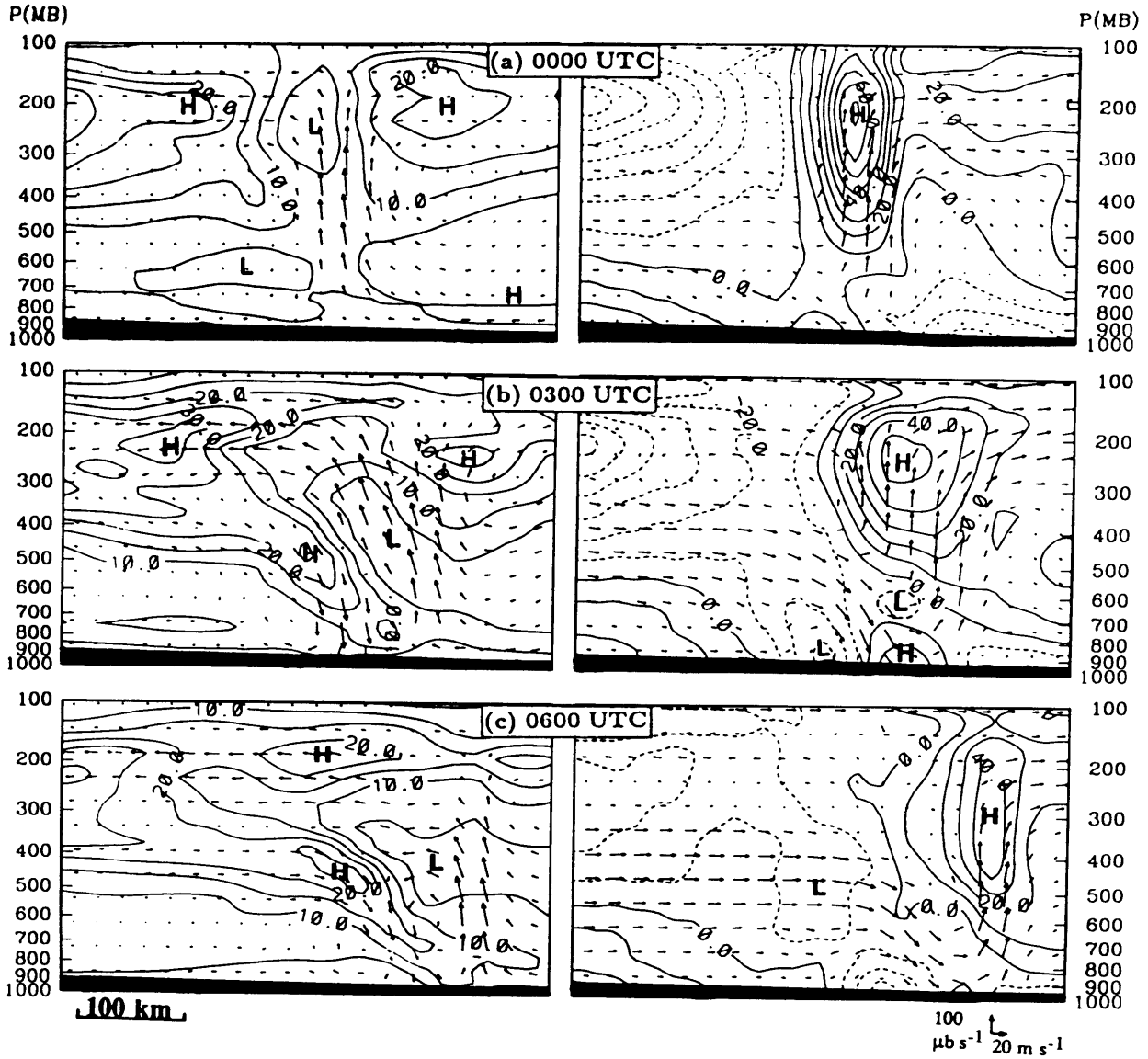

Fig. 2. Left panel shows the NW-SE vertical cross-sectional maps of total kinetic energy (K) at intervals of 5×10^4 J m^{-2} (50 mb)$^{-1}$, superposed with cross-line relative flow vectors, from 12, 15 and 18 h simulations, valid at 0000, 0300 and 0600 UTC 11 June 1985, respectively. Right panel shows the corresponding maps of height deviations at intervals of 10 m but superposed with actual flow vectors. All solid (dashed) lines denote positive (negative) values, similarly for the rest of figures. Cross sections are taken along the lines A-A′ in Figs. 1a–1c and cover a horizontal length of 450 km.

term GEN represents the generation of KE, or conversion of potential energy to KE, by cross-contour or ageostrophic flow. If the flow is downgradient, KE will be gained as a result of mechanical work done by the pressure gradient force. Otherwise, KE will be lost or converted to potential energy. The term DIS is the dissipation of KE due to subgrid-scale processes in the model. Since the PBL effects are only notable in the lowest 50 mb over convective regions (see Fig. 11 in Gao *et al.*, 1990), and since the effects of convective momentum transport were excluded in the Fritsch-Chappell scheme (see Zhang *et al.*, 1989), subgrid-scale KE dissipation is one to two orders of magnitude smaller than other terms in Eq. (1). Hence, the term DIS will not be considered in later discussion. In most observational KE analyses, however, this term is often calculated as a residual to balance other terms in Eq. (1), and thus differs in concept from the one used in the present study. The term TEN is the local change of KE in the quasi-Lagrangian coordinate, and computed as the sum of the above four energetic processes. Thus, the only errors contained in the term TEN are related to the aforementioned PBL and num erical diffusion effects.

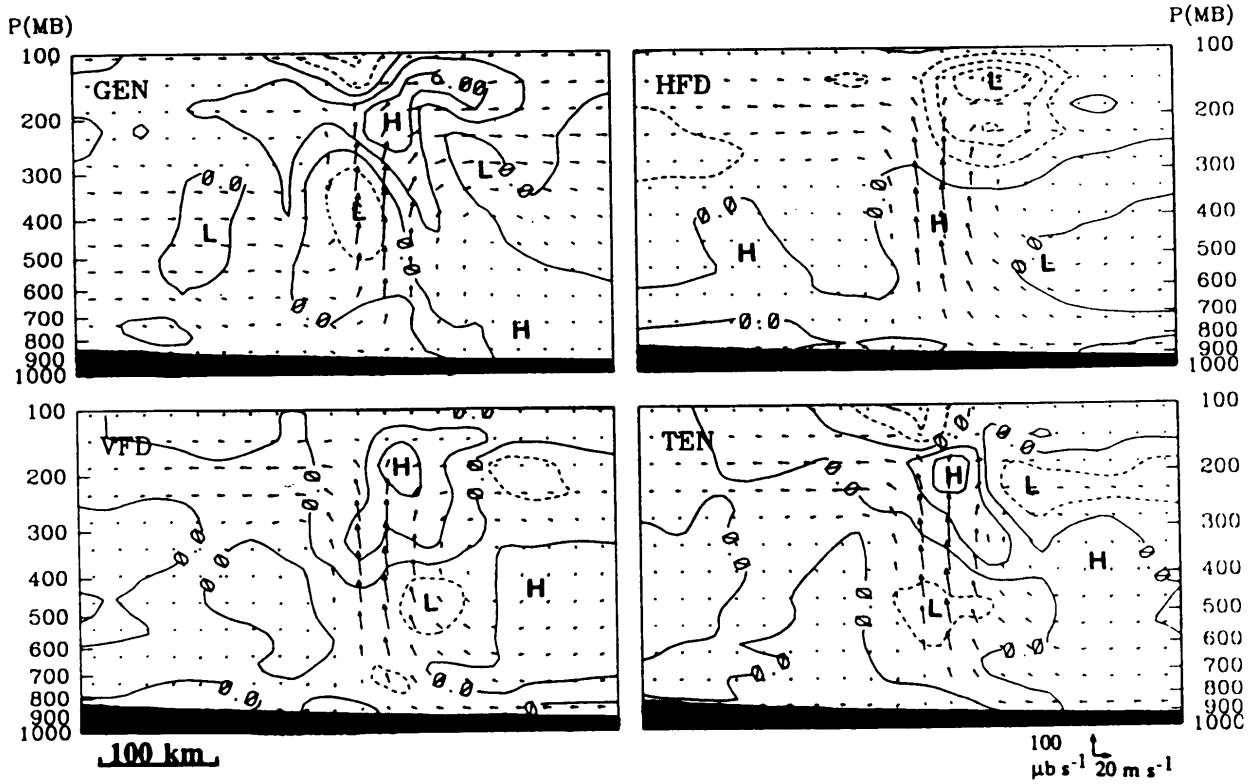

Fig. 3. Vertical cross sections of a) cross-contour generation ($\int -\boldsymbol{V}\cdot\nabla\phi$, GEN); b) horizontal flux divergence [$\int -\nabla\cdot(\boldsymbol{V}-C\boldsymbol{n})k$, HFD]; c) vertical flux divergence ($\int -\frac{\partial\omega k}{\partial p}$, VFD); and d) quasi-Lagrangian tendency ($\frac{DK}{Dt}$, TEN) at intervals of 3×10 W m^{-2} (50 mb)$^{-1}$ along the line A-A′ in Fig. 1a from 12-h simulation, valid at 0000 UTC 11 June 1985. Actual flow vectors are given in the GEN diagram whereas system-relative flow vectors are provided in other diagrams.

4. Kinetic energy budget

In this section, horizontal and vertical cross sectional maps of resolvable-scale and area-averaged KE budgets are presented to investigate the internal and mesoscale energetics of the 10–11 June 1985 squall system, as given in Fig. 2, and to describe relationships between the KE variations and the squall's internal circulation characteristics.

(a) Vertical variation of kinetic energy budget

Figures 3–5 show vertical cross sections of KE budget terms from 12, 15 and 18 h simulations, valid at 0000, 0300 and 0600 UTC 11 June, respectively. The cross sections are taken along lines to the north of the squall system and lie within a fixed vertical plane but with different segments used to follow the system (see Fig. 1). Note that overlaid with the distribution of GEN and height deviations are actual (*i.e.*, ground-relative) flow vectors, whereas in other diagrams are system-relative flow vectors. The latter will be implied in subsequent descriptions, unless otherwise mentioned.

At 0000 UTC, the squall line has formed for three hours. Figure 3 depicts that the squall's internal circulations are dominated by a FTR ascending flow and an overturning updraft during this incipient stage. Associated with the ascending motions are positive height deviations (*e.g.*, a warm-core-related mesohigh in the main updraft, see Fig. 2), which result from the latent heat release exceeding adiabatic cooling in the updrafts. As shown by Zhang and Gao (1989), the rear inflow into the squall system occurs after intense updrafts break through the large-scale RTF flow associated with the jet stream. Then this rear inflow begins to descend as sublimative and evaporative cooling takes place at the back edge of the updrafts. Thus, the ascending current tends to transport higher KE content associated with the jet stream upward, leading to positive VFD aloft and negative VFD below. However, almost all of the upwardly transported KE is offset by local negative HFD due to the presence of convectively generated strong divergent outflow near the tropopause. On the other hand, because this divergent outflow is downgradient (see Fig. 2), the GEN term provides positive contribution to the quasi-Lagrangian KE tendency in the FTR ascending region. The net result is a gain of KE and rapid intensification of the flow in the upper portion of updrafts.

By comparison, the net variations of KE in

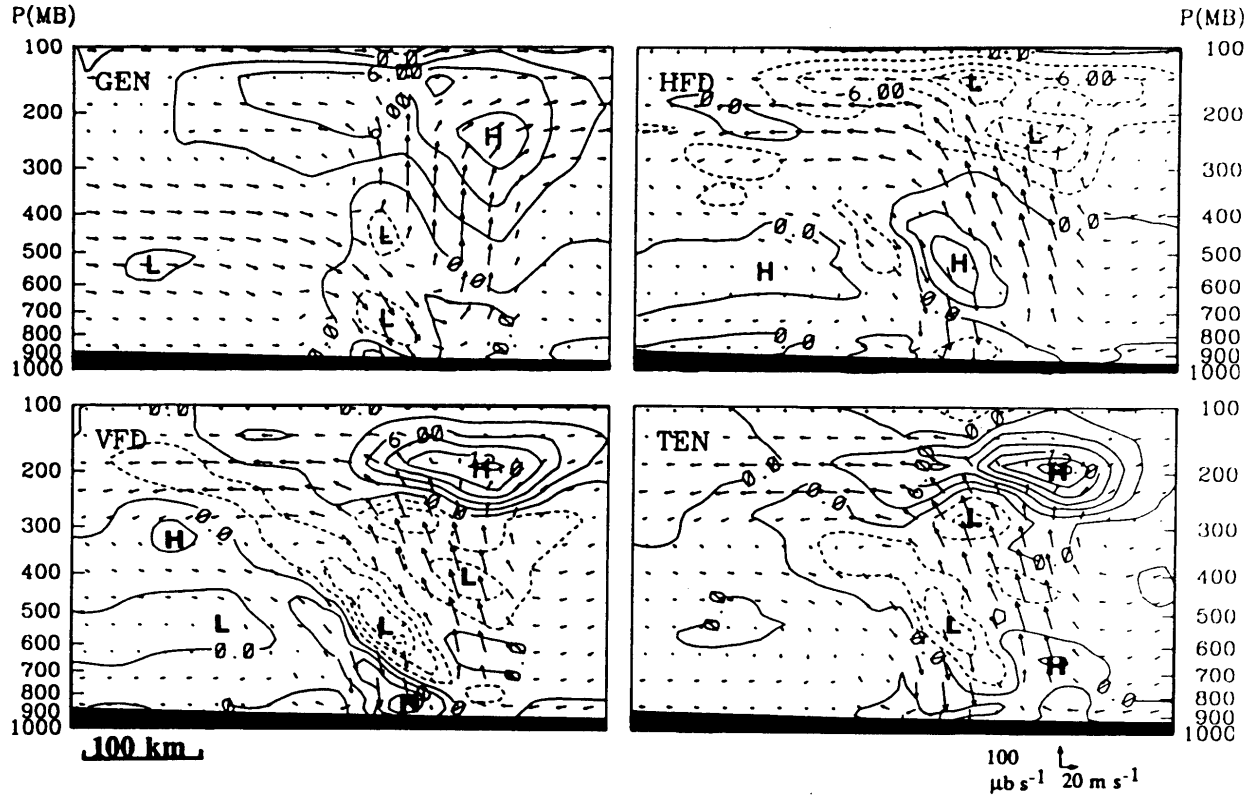

Fig. 4. As in Fig. 3 except from 15-h simulation, valid at 0300 UTC 11 June 1985.

the low-to-midtroposphere are much less significant. Specifically, although the ascending flow rapidly intensifies in response to the low-level convergence, both the HFD and VFD do not make sizable contribution to the quasi-Lagrangian tendency. These weak variation rates are attributable to the presence of a weak-gradient flow in the prestorm environment. Similarly, the efficacy of the cross-contour production is generally small, but negative in the rear half portion of the FTR ascending current. This negative KE production implies that the flow may not originate from the warm air, according to atmospheric energy theory. In fact, Fig. 2 shows that some of the air in the RTF flow appears to be forced into the updrafts in response to latent heating aloft. Hence, the actual rear inflow is "blocked" by the warm-core-related mesohigh, and becomes upgradient towards the leading updrafts. Note the little KE production by the GEN in the lowest 300-mb layer, even though significant pressure gradients have developed in association with the surface mesolows and mesohighs (see Figs. 1a and 2). This is in significant contrast with the momentum budget which shows pronounced contribution of pressure gradient forces to the intensification of the descending rear inflow across the line (see Fig. 3 in Gao *et al.*, 1990).

By 0300 UTC, the previously mentioned three air streams have become well organized, particularly the FTR ascending and RTF descending flows. Upward motion in the stratiform region as strong as 1 $m\,s^{-1}$ has developed in the presence of moist symmetric instability (see Zhang and Gao, 1989; Zhang and Cho, 1992). Thus, Fig. 4 exhibits enhanced organization and development of energetic areas that are closely related to the three air streams during this mature stage. The flow variations are also better displayed from the KE viewpoint than could be seen from the momentum budget (*cf.* Fig. 4 in Gao *et al.*, 1990 and Fig. 4 herein). In particular, the quasi-Lagrangian tendency shows substantial gains of KE in the upper troposphere over the squall-line area, and relatively smaller gains in the descending portion of rear inflow. It is evident that the cross-contour production is a source of KE in most portions of the ascending regions. This is undoubtedly a consequence of the latent heat release exceeding adiabatic cooling in the organized ascending flow, so the warmer air rises. This is consistent with the energetic theory that KE will be generated from potential energy when the warm air ascends. Furthermore, the cross-contour production appears to account for a large percentage of the net KE gain at the upper levels, especially towards the leading portion of the system (also see Fig. 3). Of great importance is that the GEN term also acts as a source of KE in the trailing stratiform region, because it indicates that the pertinent mesoscale ascent occurs in a warmer atmosphere. This result conforms to the

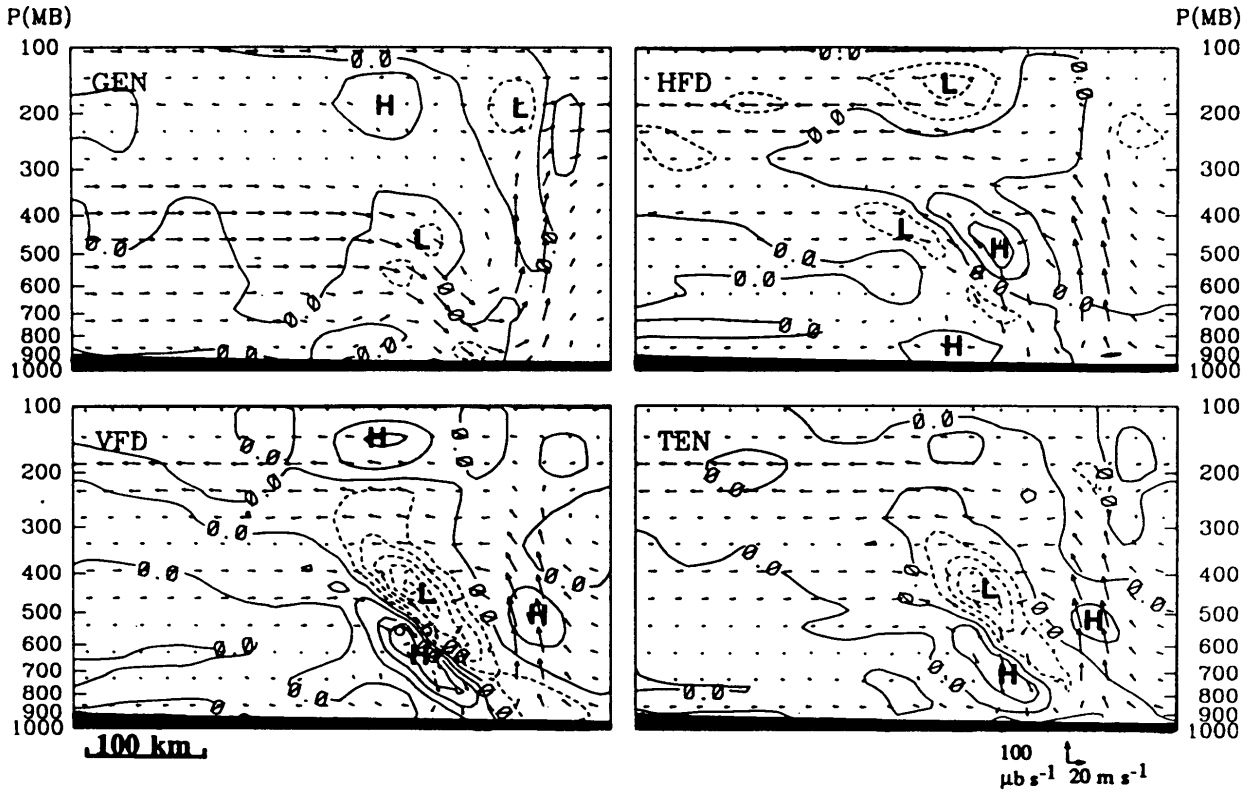

Fig. 5. As in Fig. 3 except from 18-h simulation, valid at 0600 UTC 11 June 1985.

observations that the stratiform region of MCSs often exhibits a warm-core structure (Maddox, 1983; Houze, 1989; Johnson and Bartels, 1992). Although the contribution of VFD is more significant than the GEN in the upper portion of the main updraft, most of its contribution has again been offset by the HFD within the upper divergent outflow layer. In fact, the HFD is always a KE sink in the upper troposphere during most of the squall's life cycle. The greatest quasi-Lagrangian gain of KE takes place at the top of the leading updrafts where both the GEN and VFD contributions are large. Hence, the upper-level flow should be expected to accelerate, more rapidly along the leading updrafts. This will be further shown in the next subsection.

Figure 4 also shows that the effects of the cross-contour production decrease downward due to the reduction in both horizontal winds and pressure gradients (see Fig. 2). The GEN term contributes positively, though small, to the slow increase of KE towards the flow interface in the trailing rear inflow. Of interest is that as in updraft regions at 0000 UTC (Fig. 3), the GEN acts too as a sink along the leading portion of the descending rear inflow. This indicates that the RTF descending inflow may not occur together with colder air, except ahead of the low-level cold pool where the actual flow is downgradient. With a simple numerical model, Srivastava (1985) demonstrated that the descending motion always warms the air below in a stratified flow, while the evaporation of raindrops cools it. In the present case, some portion of the descending flow could become relatively warmer as a result of the subsidence warming exceeding the evaporative cooling, especially towards the rear of the system where less condensate is available for evaporation (see Zhang and Gao, 1989). Furthermore, because the sublimative and evaporative cooling dominates along the leading edge of the descending flow, the midlevel rear inflow is in a certain sense forced to descend (Zhang, 1992). Therefore, the RTF flow above the cold pool could become upgradient, namely, in the present case, blowing from a wake low to a mesohigh pressure region (Fig. 2). Obviously, these forced warm-air descent and cold-air ascent could only occur at relatively small scales, and thus they may not be well detected by conventional observations. Nevertheless, Vincent and Carney (1984) did analyze a situation in which an airflow blew from a low to high pressure zone outside a convective storm.

The relative horizontal convergence of KE is always small in the lower half portion of the ascending flow. Only along the flow interface where both KE gradients and mass convergence are large (see Fig. 2), does the HFD show pronounced production of KE. The largest gain of KE through the HFD appears to occur above the melting level (*i.e.*, 600 mb) where the cooling-induced convergence is max-

imized (Zhang, 1992). In contrast, the effects of VFD are generally opposite in sign but more pronounced than the HFD. Given that horizontal KE in the prestorm environment increases with height up to the jet-stream level, the VFD term would act as a KE sink in the FTR ascending flow and a KE source in the RTF descending flow. Thus, Fig. 4 shows that during the mature stage the VFD overcompensates for the HFD and appears to be mainly responsible for the net loss of KE in the middle portion of the ascending flow and the net gain of KE in a deep layer behind the surface evaporatively-generated mesohigh (see Fig. 1), thereby resulting in the upwardly and downwardly tilted isopleths of KE in the respective FTR and RTF flows, and the strong gradient of KE across the interface (Fig. 2). Evidently, the downward transport of the upper-level high KE content plays an important role in determining the intensity of the descending rear inflow, as will be further seen in the next section.

By 0600 UTC, the squall system has gradually advanced into a convectively less unstable region and begun to decay (Zhang and Gao, 1989), especially for the northern portion of the line where the present cross section is taken. Hence, less latent energy is available for production of warm air in the updrafts (Fig. 5). As a result, all energetic contributions in the leading ascending regions diminish during this period. In the low- to midtroposphere, however, the squall system during this early decaying stage is dominated by organized descending motion. This is because there are still some amounts of condensate available for evaporation in the mesoscale downdrafts. Therefore, the descending regions continue to gain KE in a quasi-Lagrangian sense within a deep layer (*i.e.*, from 300 mb to the surface), due to the downward transport of the upper-level high KE content. In particular, Fig. 2 shows that at this time the isopleths of KE above 500 mb have been brought downward close to the surface by the strong RTF descending motion. This indicates that the surface gust fronts in the present case may be related through moist downdrafts to the presence of the upper-level jet stream. Because the descending rear inflow is divergent, the relative HFD exhibits negative contribution to the quasi-Lagrangian tendency; but it is overcompensated by the VFD in the presence of large vertical KE gradients. Note a narrow zone of net KE loss along the flow interface that starts to show up when the RTF descending flow becomes evident. Most of this loss is produced by the VFD, namely, any KE gain through the HFD is rapidly lost to the flow acceleration below in the descending currents. This vertical negative-positive rate couplet just reflects the downward layer-by-layer transport process of the upper-level KE content in the descending rear inflow.

(b) Horizontal variation of kinetic energy budget

To gain insight into the three-dimensional energetic variability of the squall system, Figs. 6–9 show horizontal maps of KE budget terms in relation to the squall's adjacent environment. It is also informative to examine the KE variations associated with convectively generated mesoscale rotational flow in the vicinity of the squall system. In the following, only diagrams at the mature and earlier decaying phases, in which the midlevel mesovortex and other meso-β-scale features are better developed (see Zhang *et al.*, 1989), are shown for the lower (*i.e.*, $\sigma = 0.873$ which is about 100 mb above the surface), middle (550 mb) and upper (200 mb) tropospheres. Areas with significant vertical motion are also given. Since Figs. 4 and 5 show relatively less temporal variations of KE in the low-to-midtroposphere, only upper-level maps at 0300 UTC are provided.

It is apparent from Figs. 6–9 that all significant energetic perturbations are situated behind and oriented along the squall line. In the upper troposphere (*i.e.*, 200 mb), there are large positive KE tendencies right behind the leading line, suggesting rapid acceleration of the flow after passage of the squall line. This situation is consistent with the often observed development of jet streams to the north or northwest of MCSs (*e.g.*, Fritsch and Maddox, 1981; Maddox *et al.*, 1981). For the present case, perhaps the upper-level flow structure in the immediate environment differs somewhat from that generated by a more circular type of MCSs. Specifically, the divergent outflow tends to accelerate more towards the jet stream to the north, as can be seen from horizontal flow vectors. This could be attributed to the upward transport of the southwesterly component of the jet stream from the layers below. It should be noted that the presence of a jet stream in a convective environment, as well as its strength and relative location, is extremely important in determining KE budgets at different scales. For example, Fuelberg and Jedlovec (1982) analyzed that horizontal transport of KE by jet streams could become a principle KE source to MCSs. But the jet stream in the present case renders a KE sink to the upper troposphere through the HFD, and a KE source (sink) above (below) the jet-stream level through the VFD in the ascending flow. The jet stream appears to be a major KE source in the descending rear inflow.

Note some spatial and temporal variability of the budget terms along the squall system at different development stages. During the mature phase (Fig. 6), marked cross-contour production occurs over a widespread area in the northern portion of the system where the stratiform region is located. These large values of the GEN are indicative of strong cross-angle flow from the mesohigh to its adjacent low pressure regions. Fuelberg and Printy (1984) reported that cross angles at the top of convective

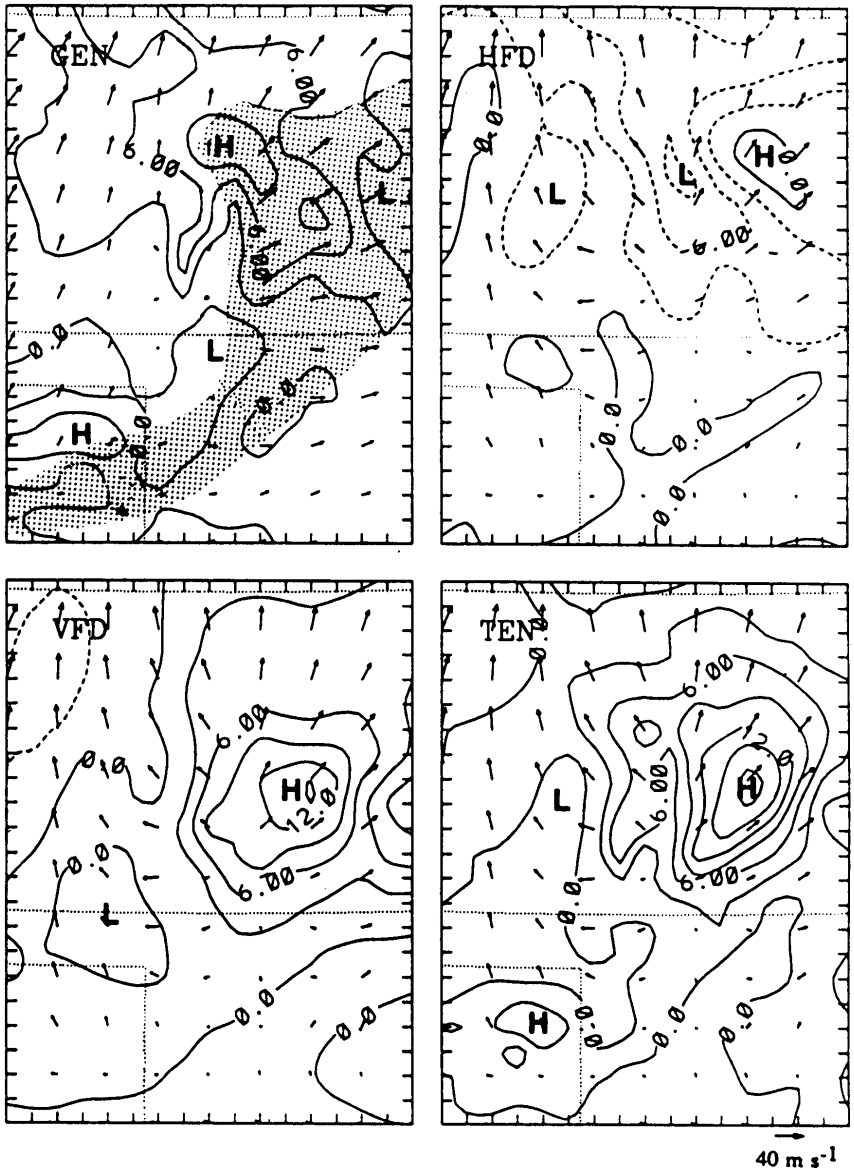

Fig. 6. Horizontal maps of a) cross-contour generation ($\int -\boldsymbol{V}\cdot\nabla\phi$, GEN); b) horizontal flux divergence [$\int -\nabla\cdot(\boldsymbol{V}-C\boldsymbol{n})k$, HFD]; c) vertical flux divergence ($\int -\frac{\partial\omega k}{\partial p}$, VFD); and d) quasi-Lagrangian tendency ($\frac{DK}{Dt}$, TEN) at intervals of 3×10 W m^{-2} (50 mb)$^{-1}$ at 200 mb over a subdomain from 15-h simulation, valid at 0300 UTC 11 June 1985. Flow vectors given in the GEN diagram are relative to the ground and in other diagrams are relative to the system. Shadings and hatchings represent the distribution of more significant up- and down-drafts, respectively.

regions could be as great as 90^0, as also seems to be the case herein. When the system enters the decaying phase, the stratiform precipitation expands into a much greater area behind the leading updrafts (*cf.* Figs. 6 and 7). Meanwhile, the low-level southwesterly energy supply is interrupted by deep convection to the south of the line (see Fig. 9 herein and Fig. 3 in Rutledge *et al.*, 1988). Thus, the upward motion to the north begins to weaken, and the effects of GEN and VFD decline. The GEN even becomes a sink of KE to the north of the system where upward adiabatic cooling may exceed local latent heating (Fig. 7). As the center of updrafts is displaced to the southwest, so is the influence of cross-contour flow and upward KE transport. Since these two processes always overcompensate for the HFD over the convectively active regions, net gain of KE prevails to the southwest of the line. This results in the marked contrast between the convectively generated divergent outflow and the environmental flow. In essence, the squall system moves progressively into a weak flow region toward the southeast, and leaves behind an enhanced south to southwesterly flow. This divergent outflow clearly plays an important role in

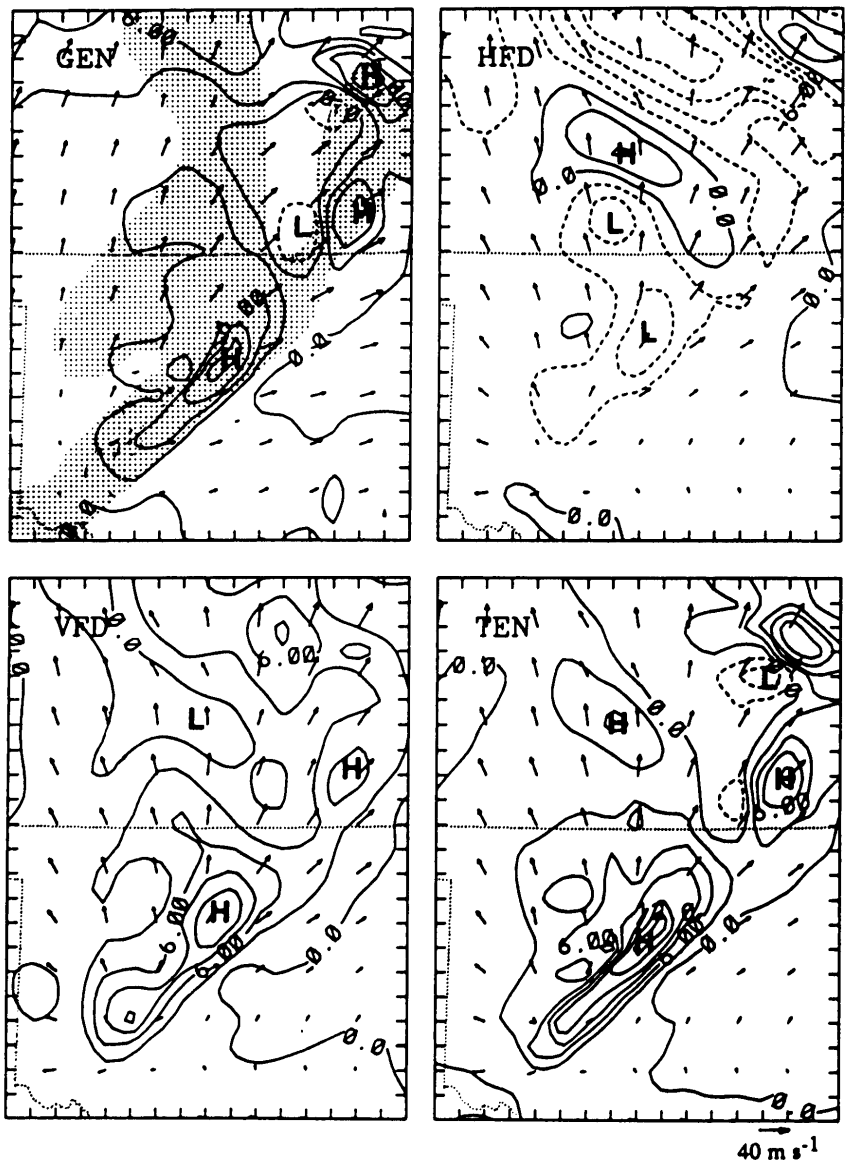

Fig. 7. As in Fig. 6 except from 18-h simulation, valid at 0600 UTC 11 June 1985.

the formation of a large stratiform region behind the leading line.

At 550 mb (Fig. 8), a midlevel mesovortex has become well developed beneath stratiform clouds during the mature and decaying stages (see Zhang, 1992). Although the squall's circulations are three dimensional in character due to the presence of the mesovortex, all energetic influences at the midlevels are mainly determined by the squall's vertical motion and occur linearly along the system. The cross-contour flow produces notable destruction of KE along the leading portion of the descending rear inflow, as previously mentioned. But the GEN contributes positively to the quasi-Lagrangian tendency elsewhere, particularly in the ascending flow during the system's intensifying phase (*cf.* Figs. 4 and 8). The HFD term also causes destruction of KE in the divergent descending flow but generation of KE in the convergent ascending flow with the strongest amplitude occurring along the interface. Nonetheless, the VFD appears to determine the net gain of KE in the trailing RTF flow and the net destruction of KE along the leading edge due to the loss to the flow below. Thus, the downward transport of the upper-level KE and the combined effects of the GEN and the HFD are responsible for the intensification of west-to-northwesterly and south-to-southeasterly components of the vortex circulation, respectively. Evidently, the strengthening of the RTF descending flow enhances the midlevel mesovortex via both tilting and stretching (see Zhang, 1992).

In the lower troposphere, the divergent descending outflow is seen vertically sloping downward from 400 mb and now occupies a larger area than the as-

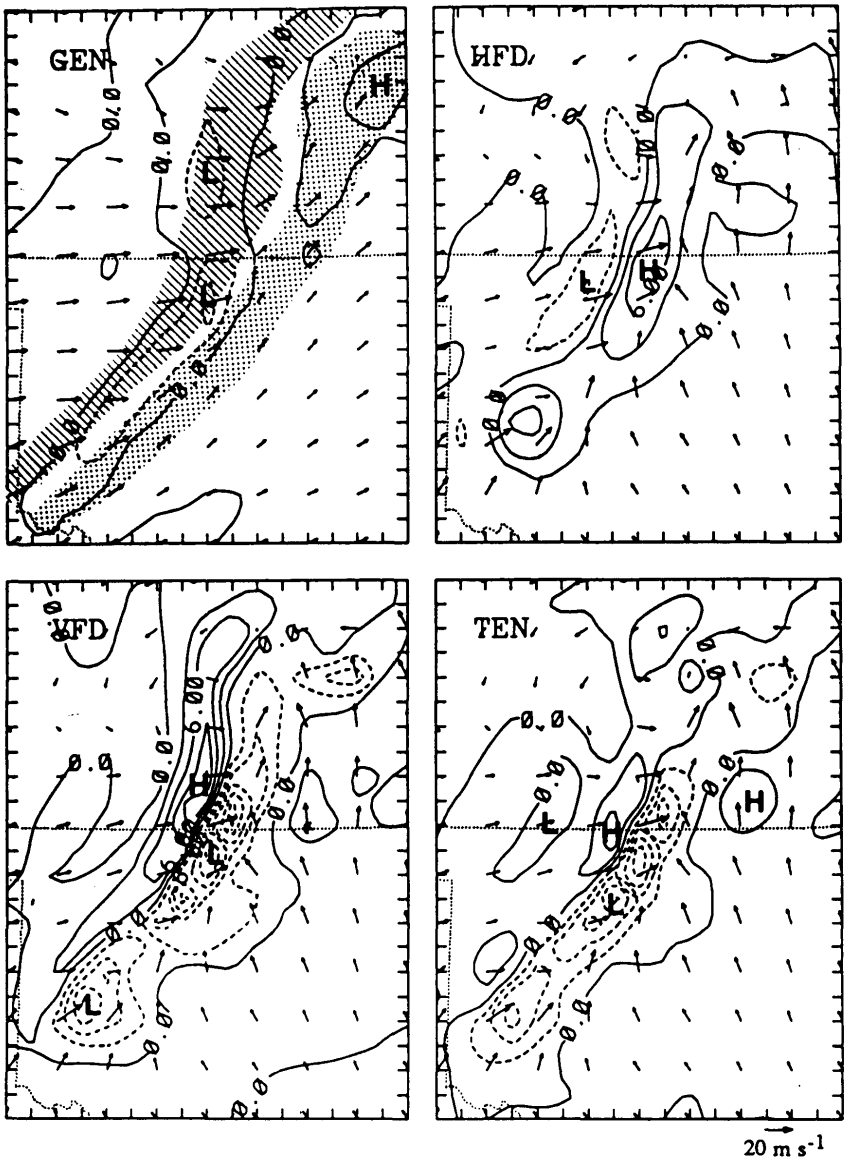

Fig. 8. As in Fig. 6 except at 550 mb from 18-h simulation, valid at 0600 UTC 11 June 1985.

cending motion along the leading line (see Figs. 5 and 9). Because of the strong descending flow, the downward transport of midlevel KE becomes the dominant source of KE behind the squall line. This leads to the development of northeasterly flow in the system's wake, since the upper-level cold air tends to subside anticyclonically, *e.g.*, from southwesterly at upper levels to westerly at midlevels and northeasterly at low levels (see Figs. 7–9). Unlike the generation term in the horizontal momentum equations, the presence of mesohighs and mesolows in the lowest layers again does not seem to have significant contribution to the KE budget through the GEN, except ahead of the leading line where the ground-relative flow has intensified.

(c) Temporal variability of composite energetics

After showing the detailed structure of energetic processes, it would be of interest to examine the time evolution of mesoscale KE budgets that are averaged over a box of 250 km (along-line) × 150 km (across-line) following the squall system during its life cycle. Figure 10 displays that the vertical distribution of the area-averaged budgets is generally similar to that analyzed from the vertical cross sections in Figs. 3–5. But their magnitudes are much smaller than those described earlier, as expected. Perhaps of most significance is that many detailed energetic processes in the low to midlevels have been filtered out after area averaging, especially those associated with moist downdrafts. One exception is during the decaying stage in which evaporatively driven downdrafts prevail within the system. In contrast, most energetic processes happened in the upper troposphere are well captured. This is because the upper-

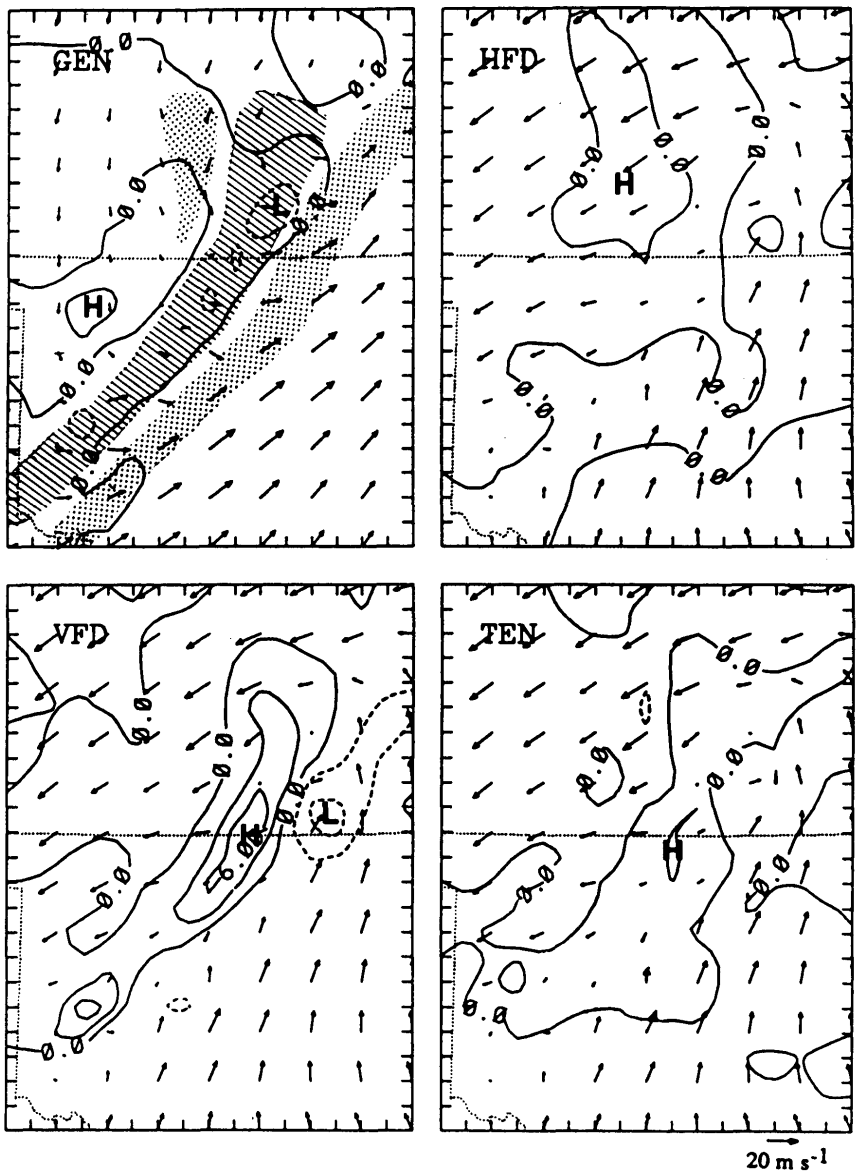

Fig. 9. As in Fig. 6 except at a level about 100 mb above the surface (*i.e.*, $\sigma=0.873$) from 18-h simulation, valid at 0600 UTC 11 June 1985.

level divergent outflow occurs at a scale much larger than the concentrated updrafts below (Fritsch and Brown, 1982); in the present case it has a scale of 300–400 km (*cf.* Figs. 3–5).

It is apparent from Fig. 10 that the cross-contour generation, even averaged over a mesoscale area, is still the major source of KE to the upper troposphere. The VFD is a secondary KE source above the jet-stream level; but most of its contribution is offset by the HFD in this divergent outflow layer. Below the jet-stream level, the upward transport of lower KE in the prestorm environment is responsible for the net destruction of KE in the midtroposphere. These basic scenarios persist during the incipient and mature stages of the squall system, although there is some temporal variability in magnitude. All energetic processes diminish once the system begins to dissipate.

Figure 11 shows a time series of vertically integrated KE budget terms, based on the results from Fig. 10. The time evolution of the VFD is not given, because its vertical integration from the surface to the model top vanishes. After all, the VFD only plays a role in vertically redistributing KE through FTR updrafts and RTF downdrafts. As can be seen, the column-integrated quasi-Lagrangian KE tendency increases steadily during the intensifying period, and then drops rapidly as the system decays. This KE evolution is primarily determined by the cross-contour production of KE resulting from the net heating of the atmospheric columns (see Fig. 20 in Zhang and Gao, 1989). In contrast, the

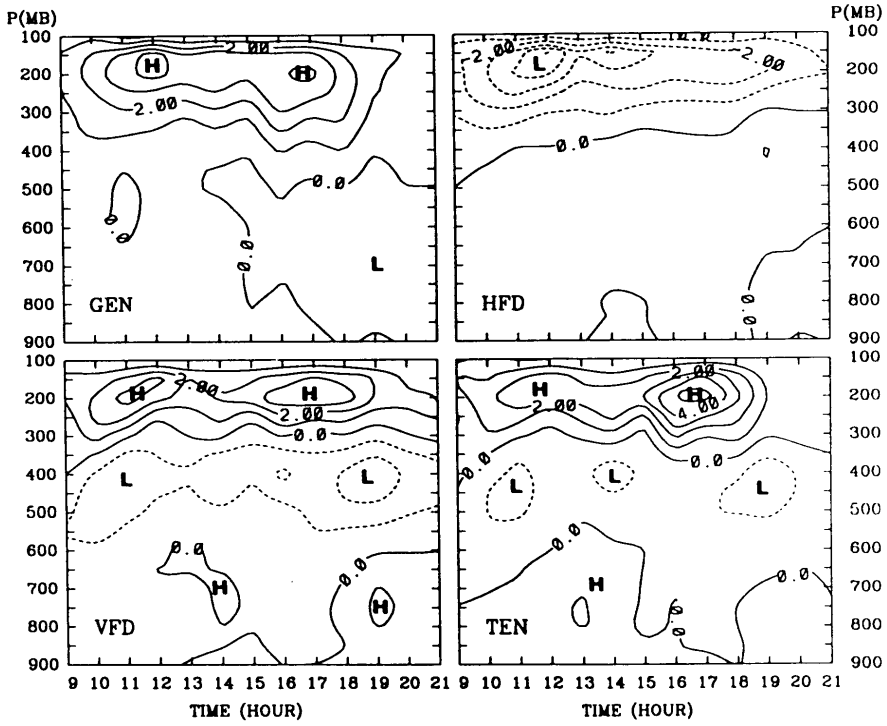

Fig. 10. The time evolution of area-averaged (250 km × 150 km) vertical profiles of a) cross-contour generation ($\int -\boldsymbol{V}\cdot\nabla\phi$, GEN); b) horizontal flux divergence [$\int -\nabla\cdot(\boldsymbol{V}-C\boldsymbol{n})k$, HFD]; c) vertical flux divergence ($\int -\frac{\partial\omega k}{\partial p}$, VFD); and d) quasi-Lagrangian tendency ($\frac{DK}{Dt}$, TEN) at intervals of 10 W m^{-2} (50 mb)$^{-1}$, following the movement of the squall system.

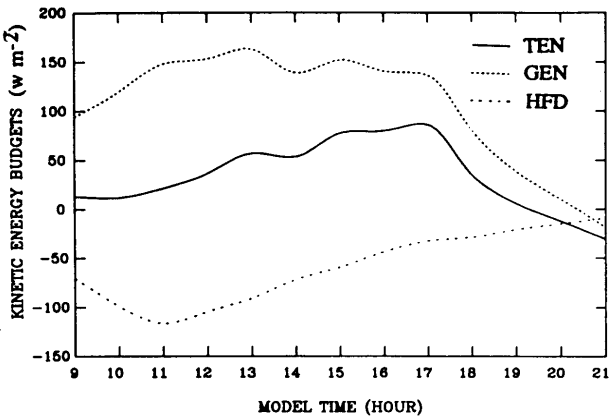

Fig. 11. The time evolution of vertically integrated and area-averaged kinetic energy budgets that are obtained from the results given in Fig. 10.

vertically-integrated HFD becomes a major sink of KE to the squall system that counteracts with the cross-contour production. Of course, the vertically-integrated frictional effect is also a non-conservative sink to the total KE of the system (see Lin and Coover, 1988; Lin *et al.*, 1991). Obviously, the cross-contour generation will be the only non-conservative source to the system, when the KE budget equation is evaluated over a sufficient large area.

(d) Comparison with previous studies

It is evident from the above KE analyses that the energetic processes of the simulated squall system vary greatly from its adjacent environment to the storm region, from updrafts to downdrafts, and from the lower to upper troposphere. The high-resolution simulation data permit a detailed view of the meso-β-scale variability of the squall-line's energetics. None of previous observational studies could reveal the energetic variability of an MCS and its relationships with the MCS's internal and adjacent flows, owing to inadequate data. In particular, little have been presented on the KE budgets associated with the descending flow in the stratiform region. Thus, it is not practical to make quantitative comparisons between our results and previous KE budget analyses. Nevertheless, it is still possible to qualitatively compare our budgets for the MCS itself with those of MCS' environment, even though there are some differences in data sources, grid resolution, and the type and severity of MCSs. Specifically, current results are most similar to those of Fuelberg and Printy (1984) for a KE budget of the meso-β-scale near-storm environment using the rawinsonde observations at 75 km spacing and 1.5 h intervals. Their composite area-time averaged budgets do show more significant variations at the upper levels with the GEN and VFD terms as the main sources of KE and the HFD and DIS terms as the major sinks (see

their Fig. 5). At the low-to-midlevels, the budget terms show weak but opposite contribution to the KE balance equation. The largest contribution of these terms appears near the jet-stream level (*i.e.*, around 200 mb). However, the average magnitudes of the upper-level GEN, HFD and VFD contribution inside the MCS are generally 2, 3 and 8 times, respectively, greater than those in the MCS' immediate environment. The more pronounced difference in the VFD contribution is clearly caused by the grid spacing of rawinsonde observations that often fails to detect more intense circulations. The grid resolution problem also appears to explain some other pronounced differences. For example, the Fuelberg and Printy study, as well as others (*e.g.*, Tsui and Kung, 1977; Vincent and Schlatter, 1979), shows substantial net KE loss at the upper levels in the vicinity of the MCS being studied. This KE loss results primarily from the dissipation that is obtained as a residual of the KE balance equation; and thus it is associated with the processes that are not adequately resolved by the observational network. In the present study, however, the dissipation effects are only associated with numerical diffusion and the PBL processes. Thus, many internal energetic elements shown in Figs. 3–9 would be either treated as the subgrid-scale dissipative processes or aliased into larger-scale features in mesoscale observational studies. Nevertheless, the above comparisons suggest that the current observational network could only depict the basic influence of MCSs on the larger-scale environments above the concentrated updrafts, because their most significant energetic effects occur in a thin layer in the upper troposphere; but it may fail to represent the energetic effects of downdrafts.

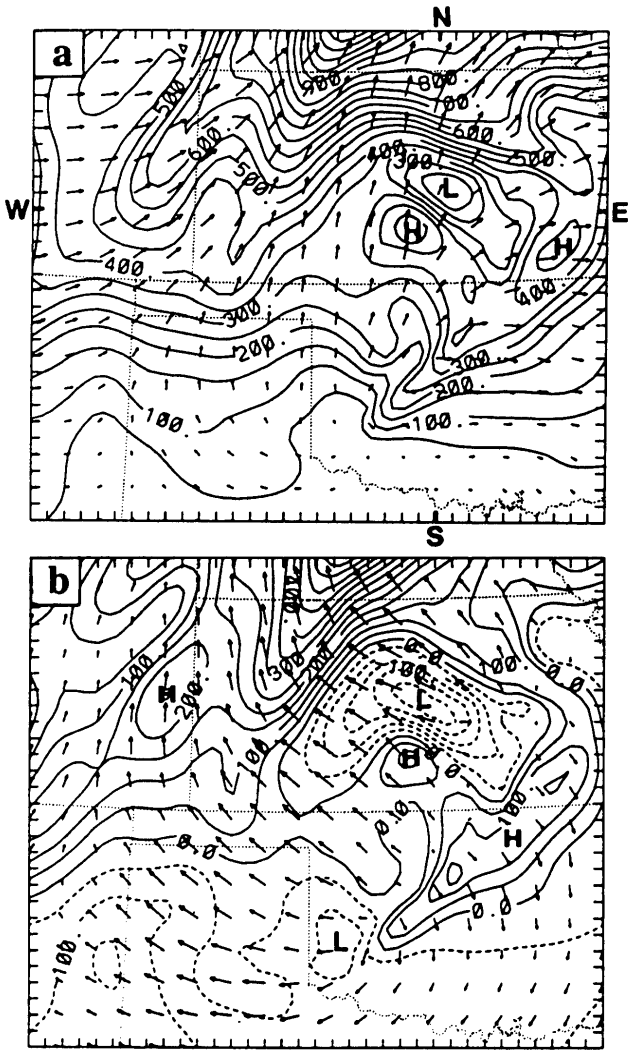

Fig. 12. Distribution of 200-mb a) horizontal kinetic energy, superposed with actual flow vectors; and b) kinetic energy deviations between the control and NDH (no diabatic heating) runs, superposed with deviation flow vectors, at intervals of 50 J kg^{-1} over a large domain from 18-h simulation, valid at 0600 UTC 11 June 1985. Letters 'W-E' and 'S-N' denote the location of vertical cross sections used for Figs. 13 and 14, respectively.

5. Energetic effects of the squall line

As with observational KE analyses, the budget results presented above include energetic effects of all scales on their larger-scale flow. To isolate the convective effects, an additional numerical experiment was run, in which neither parameterized convection nor grid-scale condensational heating (Exp. NDH) was included (see Zhang and Fritsch, 1988). This simulation presumably produces the evolution of the large-scale basic state without the influence of the squall system. Thus, any KE deviations between the control run and Exp. NDH could be attributed to the development of the squall system. These two sets of data are analyzed in both a physical and a wavenumber space and discussed below.

(a) The net effects of the squall system

The control-simulated KE distribution and the KE deviations at 200 mb near the end of the squall's life cycle are given over a larger subdomain in Figs. 12a and 12b, respectively, which exhibits significant perturbations everywhere over the subdomain, being more pronounced behind the squall line. The squall region first experiences a rapid KE increase northeastward along the leading updrafts, and then a slow increase over the stratiform region. Although there are some negative deviations in the northern portion of the stratiform region, which result from the weakening of local FTR ascending flow during this decaying stage (*cf.* Figs. 7 and 12), the substantial intensification of southwesterly flow and KE gradients to the north and northwest of the squall system is clearly apparent. The largest KE content

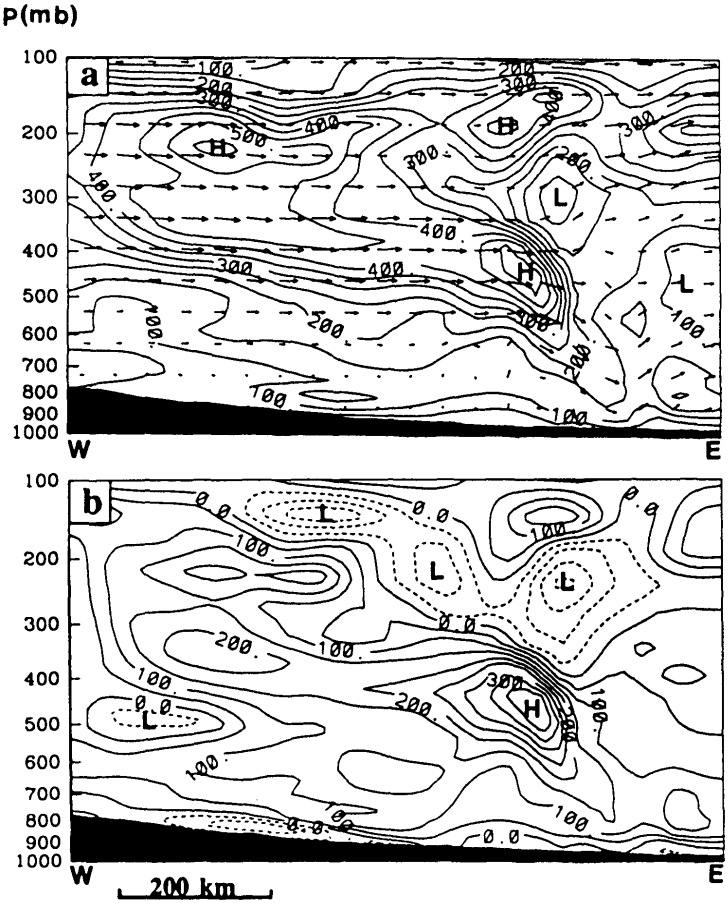

Fig. 13. West-east vertical cross sections of a) horizontal kinetic energy (k), superposed with W-E vertical circulation vectors relative to the ground; and b) kinetic energy deviations between the control and NDH (no diabatic heating) runs at intervals of 50 J kg^{-1} from 18-h simulation, valid at 0600 UTC 11 June 1985. The location of the cross section is given in Fig. 12a.

exceeds 1800 J kg^{-1} (see Fig. 14a), which is equivalent to a wind speed of 60 m s^{-1}. This is obviously a consequence of the "obstacle" effects of the squall system (Fritsch and Brown, 1981). Specifically, the KE budget analysis shows that the upper-level flow over the squall region is driven by the squall's internal circulations. This can be further evidenced by the distribution of convectively generated deviation flow (see Fig. 12b), which displays characteristic across-line divergent outflow over the squall region and general anticyclonic flow outside. Note that this flow pattern is distinct from a circular type of anticyclonic outflow associated with mesoscale convective complexes (*e.g.*, see Fig. 6 in Zhang and Fritsch, 1988; and Fig. 20 in Maddox *et al.*, 1981). In addition, the continuous KE production and transport into the upper troposphere also help enhance the outflow downstream, leading to the acceleration of the jet stream and extremely large KE deviations to the northwest (see Fig. 12b). Of significance is the area of convective influences that more than doubles the active portion (*i.e.*, with significant vertical motion) of the squall system. However, the simulation shows only slight west-east oscillations with a monotonic increase of KE content towards the jet stream to the north (not shown), when the diabatic heating was turned off (*i.e.*, Exp. NDH).

To see how the entire model troposphere is affected by the development of the squall system, Figs. 13 and 14 show the west-east and south-north cross sections, respectively, of the control-simulated KE content and the KE deviations. It is evident that the squall system disturbs a deep layer in the troposphere. The net convective effects are most pronounced within a layer of 250 mb in the upper troposphere and increase northward, as also indicated by the KE budgets. The upper-level weak and negative deviation regions to the south represent the convective "blocking" effects through the FTR ascending flow. Next, large KE values are distributed along the trailing descending RTF flow (over a distance of > 600 km); most of these values appear to be transported downward from the jet stream. Zhang and Gao (1989) and Zhang (1992) mentioned that the

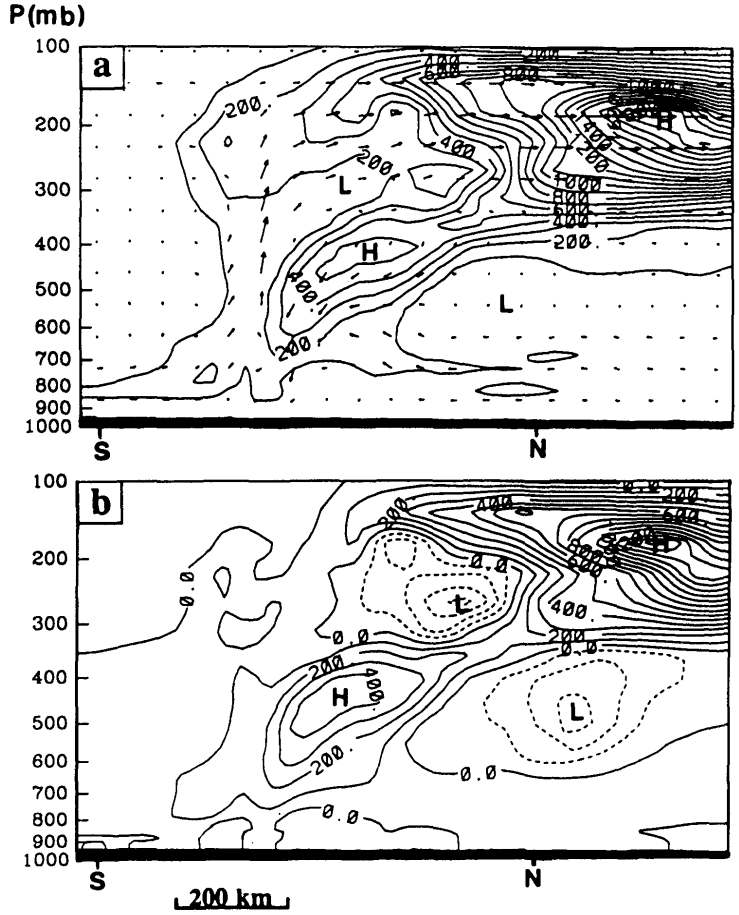

Fig. 14. As in Fig. 13 but for south-north vertical cross section at intervals of 100 J kg^{-1}, superposed with S-N vertical circulation vectors relative to the ground. The cross section is taken across the fine-mesh domain with the letters 'S' and 'N' denoting the location of the subdomain's S-N boundaries in Fig. 12a, respectively.

presence of a cross-line component of the jet stream along with a dry upper troposphere tends to provide a favorable condition for the development of the RTF descending flow. It has been shown herein that the downward transport of the jet stream KE accounts for a large percentage of the positive KE deviations in the low to midtroposphere, since both the GEN and HFD produce destruction of KE in most portion of the descending flow, except near the surface cold pool and the flow interface (see Figs. 3–5). Because the volume of the divergent descending flow increases downward, the magnitudes of the associated KE content and deviations decrease as approaching the surface (*cf.* Figs. 8, 9, 13 and 14).

Of striking interest is that the presence of the jet stream appears to affect the intensity of surface gust fronts several hundreds kilometers away not only to the front but also to the southwest of the system (Fig. 14). Note that most of the jet-stream KE content occurs along the line (see Fig. 12), rather than across the line. Otherwise, the dynamical structure of the squall system could be markedly different (Rotunno *et al.*, 1988). As an aid in understanding the energetic influences of the jet stream, Fig. 15 shows the portion of enhanced KE deviations associated with the descending rear inflow at various levels. The area of concentrated deviations is displaced downward from the northwest near the jet-stream level to the southwest of the squall system at the lower levels. Meanwhile, the upper-level southwesterly flow turns into westerly at the middle levels, northwesterly at 700 mb and northeasterly below (see Figs. 7–9 and 15), as it descends anticyclonically towards the surface over a horizontal span of more than 400 km and a depth of 550 mb. Quantitatively, an air parcel following the RTF descending flow will increase its northeasterly component by 10 m s^{-1} for every 100 km across-line displacement in accordance with the angular momentum conservation principle, assuming the Coriolis parameter of 10^{-4} s^{-1}. Such scenarios could also been seen from trajectory calculations (see Fig. 11 in Zhang and Gao, 1989). Clearly, the intensification of the low-level northeasterly flow tends

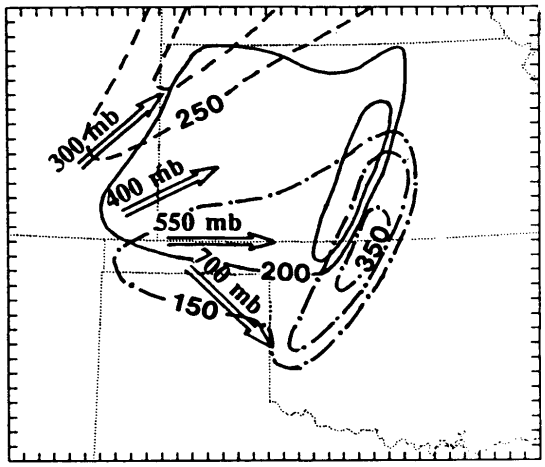

Fig. 15. Distribution of concentrated kinetic energy deviations at intervals of 100 J kg^{-1} that is associated with the descending flow in the trailing stratiform region at 300 mb (dashed), 400 mb (solid) and 550 mb (dot-dashed) from 18-h simulation, valid at 0600 UTC 11 June 1985. Arrows indicate the prevailing flow directions at these levels.

to enhance convergence for continued convective development to the southwest (see Figs. 1 and 14a). Hence, the downward KE transport along the line should be regarded as being of equal importance to that across the line, when the earth rotational effect is included. The result reveals an important mechanism whereby an upper-level jet stream could affect the evolution of MCSs through the RTF descending flow, besides the mass adjustment process shown by Uccellini and Johnson (1979). Perhaps it is appropriate to state that the mass-adjustment process provides a favorable secondary circulation for the initiation of MCSs, whereas the vertical KE transport helps strengthen the RTF descending flow and affect the further evolution of the MCSs. The downward KE transport would be more significant through sublimative and evaporative cooling when large amounts of stratiform precipitable particles could be deposited into the jet stream. This indicates that certain model physics, such as ice microphysics and explicit moisture schemes, are instrumental in the generation of the stratiform precipitation, descending flow and surface pressure perturbations, in addition to the parameterized downdrafts (Zhang *et al.*, 1989; Zhang and Gao, 1989; Zhang, 1992). In fact, Zhang and Gao (1989) showed that the RTF descending flow becomes very weak, when the diabatic cooling processes were omitted in the model (see their Figs. 13 and 15). The result also suggests that our current knowledge on the effects of convectively generated downdrafts, particularly for parameterization in larger-scale models, needs to be revised. Specifically, the mesoscale descending flow in midlatitudes should be viewed to occur anticyclonically along three-dimensional slantwise surfaces, like the FTR ascending flow (Zhang and Cho, 1992), rather than just within a vertical column or a two-dimensional vertical cross section.

Note the dipole structure of KE deviations centered around 500 mb that represents the energetic impacts of the convectively generated mesovortex on the larger-scale flow (Fig. 14b). The influence of the associated rotational circulation is as large as 600–800 km along the line and 300–400 km across the line, again much greater than the active portion of the squall system. As shown by Zhang (1992), this midlevel mesovortex is induced by diabatic cooling in the RTF descending flow, and amplified through tilting of horizontal vorticity during the intensifying stage and stretching during the decaying stage. Apparently, the mesovortex influences the environmental flow by slowing down the southwesterly winds underneath the jet stream to the north while accelerating the RTF flow to the south (Fig. 14). On the other hand, the intensification of the RTF flow and the FTR return flow would assist the concentration of cyclonic vorticity associated with the vortex (see Zhang, 1992). Since the return flow of the vortex is relatively warm and moist, it tends to ascend slowly rearward. Thus, the relative RTF flow to the north fails to reach the surface (*e.g.*, see Fig. 5 in Zhang and Gao, 1989) or may reverse its direction when the return flow is strong. This implies that more widespead rainfall but less violent weather events may occur to the north beneath the jet stream than to the south, as happened in reality (Johnson and Hamilton, 1988). It is apparent that with the development of the mesovortex, the squall line circulations should be viewed in a three-dimensional framework, rather than in two dimensions (Houze *et al.*, 1989).

(b) Kinetic energy spectra

Because of the importance of mesoscale flow for analyses of energy transfer, there has been considerable interest during the past decades in the mesoscale KE spectra (*e.g.*, Gage, 1979; Lilly, 1983). Specifically, a wavenumber k^{-3} distribution has been derived by Charney (1971) and verified by Chen and Wiin-Nielson (1978) for two-dimensional flow with wavelength between 1000 and 3000 km. A $k^{-5/3}$ distribution has been found to be suitable for three-dimensional flow with wavelength less than 1 km (Kolmogorov, 1941), and recently extended by Nastrom and Gage (1985) up to 400 km. However, much remains to be understood about the form of the spectrum between the two extremes of wavelength, particularly when convective effects are included.

To examine the spectral characteristics of con-

vective effects, the simulated wind data along the model-x direction across the coarse-mesh domain (*i.e.*, 3600 km × 3000 km) are smoothed using the 1-2-1 filter and detrended following Errico (1985). Then a Fourier transform is applied, and the sums of the squares of the Fourier coefficients at each wavelength are longitudinally averaged over 750 km (*i.e.*, 30 rows) where the squall's influence is more evident. The results for both the NDH (thin-solid lines) and control (thick-solid lines) runs are given in Fig. 16, which shows the upper-level (*i.e.*, 200 mb) and the lower-level (*i.e.*, $\sigma=0.873$ that is about 100 mb above the surface) spectra over the wavelength range from the model resolvable scale (*i.e.*, 50 km) to the domain size (*i.e.*, 3600 km). Midlevel spectra are not shown because they have intermediate structures between the upper- and lower-level spectra. As can be noted, there are some wiggles in the central portion of the spectra; they are attributable to the limited rows of spectra used for average. Nevertheless, it is noted that the model produces approximately a -3 KE spectrum for wavelength longer than 500 km and a $-5/3$ spectrum for wavelength less than 150 km in the upper troposphere from Exp. NDH (Fig. 16a). This implies that the simulated spectra have roughly the shape expected from the theory of quasi-two-dimensional turbulence and the theory of buoyancy waves (Gage, 1979; Lilly, 1983). By comparison, the KE spectrum in the lower troposphere still exhibits the $-5/3$ slope for shorter wavelength, but a close to -2 slope for longer wavelength. Moreover, the spectral magnitudes for larger scales are smaller than their counterparts in the upper troposphere. These spectral shapes are of little interest otherwise since they are attributable to the initial and lateral boundary conditions being used. They are discussed here because of our interest in the effects of the MCS on the spectral distribution of KE.

Specifically, when the diabatic heating effects are incorporated, spectral amplitudes show increases at all wavelengths longer than 150 km from the lower to upper troposphere, except on the model domain scale at which spectral amplitudes for both the control and NDH runs are constrained by the same lateral boundary conditions. The largest increase occurs between 1000 and 2000 km in which the convectively generated spectral amplitudes more than double that in Exp. NDH. Of special interest is that there are little variations in spectral shape and amplitude at shorter wavelengths, even though the simulated squall system exhibits disturbances at different scales down to the grid resolvable scale. This finding appears to differ from the controversial view that a spectral peak should be expected near the squall scale because of the concentrated KE contents at the MCS scale. To help understand the spectral characteristics of moist convection, Figs. 16a, 16b also provide the KE variances (dot-dashed lines), that are computed from the deviation winds between the control and NDH runs, and the total KE spectra (dotted lines) that are obtained by superposing the variance amplitudes with that from the NDH. First, the KE variances at both the upper and lower levels do not display any peak within the present wavenumber domain, even though Figs. 12 and 13 show the squall-related KE concentration occurring around the wavelength of 500–1000 km. Instead, longer wavelength tends to have larger variance amplitude, even if the wavelength domain were extended to an extremely large scale. Second, despite some differences in amplitude at certain wavelengths, the basic structure of the total KE spectra resembles the control-simulated, again with no peak at any intermediate scales. This indicates that the differences in spectral amplitude between the control and NDH runs represent the net effects of the squall system on different scales of motion. Then, it follows that the convectively intensified spectral amplitude at longer wavelengths could not be viewed as the upscale KE propagation or "the reverse energy cascade," as discussed by Gage (1979) and Lilly (1983). These amplitude increases are simply a consequence of the intermittent development of deep convection over the wavelength domain. In other words, a peak for either the KE variances or the KE spectra may appear near the squall-system scale if the MCS occurs periodically across the domain. If this is true, we may not likely obtain a mesoscale spectral peak in the presence of MCSs, because MCSs seldom develop periodically in midlatitudes.

6. Concluding remarks

A meso-β-scale KE analysis was performed for a life cycle of a midlatitude MCS, using a 21-h real-data simulation of an intense squall system that occurred during 10–11 June 1985 PRE-STORM. It is found that the squall's internal airflows have important impacts on the KE structures within the system and in its adjacent environment. On the other hand, the prestorm KE distribution and the convective redistribution of KE affect the intensity of the squall's internal airflows. Results show that (i) the cross-contour generation acts as a major source of KE in the FTR ascending flow and a weak source in the trailing rear inflow; (ii) the horizontal flux divergence is mainly a KE sink in the divergent upper troposphere; and (iii) the vertical flux divergence is a sink (source) in the FTR ascending flow below (above) the jet-stream level, but it is always a source in the RTF descending flow. When the KE budgets are evaluated over a sufficient large area, the cross-contour production becomes the only nonconservative KE source to the squall system as a result of the net heating of the atmosphere. It is found that the squall system has an important "blocking" effect on its environmental flow, particularly

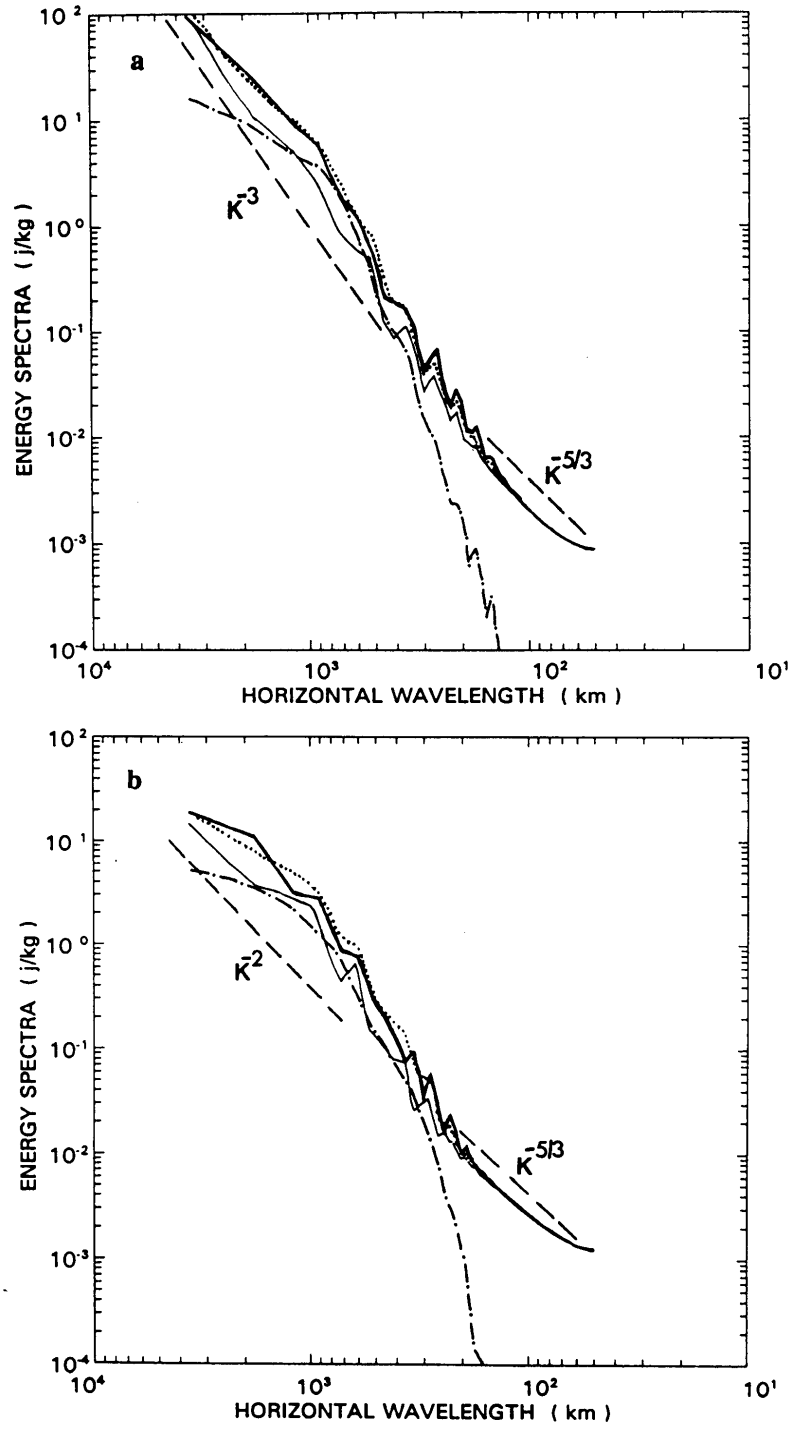

Fig. 16. Horizontal kinetic energy spectra ($J\,kg^{-1}$) averaged over 750 km for the wavelength range 50 to 3600 km at a) 200 mb; and b) $\sigma = 0.873$ (*i.e.*, about 100 mb above the surface). Thick-solid and thin-solid lines denote the spectrum from the control and NDH (no diabatic heating) runs, respectively. Dot-dashed lines represent the KE variance and dotted lines denote the sum of the NDH spectral and the variance amplitudes.

through the FTR current in the middle to upper troposphere. The development of a midlevel mesovortex tends to enhance the RTF flow to the south while slowing down the westerly winds underneath the jet stream to the north. The results agree qualitatively with some of the previous mesoscale KE analyses, and indicate that the current observational network could provide the qualitative influence of MCSs on their larger-scale environments in the upper levels, but may miss the effects of downdrafts in the lower

half portion of the troposphere.

In this study, it has been documented that the presence of an upper-level jet stream with most of the KE content occurred along the line could enhance the intensity of the RTF descending flow via the downward KE transport, and then affect the evolution (*e.g.*, the low-level convergence) and the internal airflow structure (*e.g.*, the strength of the midlevel mesovortex) of MCSs. This argument appears to help explain partly why the RTF flow in the present case is so strong and the squall system is so well organized. The results also indicate the importance of incorporating realistic physical representations into mesoscale models, such as cloud and ice microphysics, in order to reproduce well the interaction of MCSs with their environmental flow, and the pertinent internal airflow structures and evolution.

The KE spectral analysis shows that including the effects of the squall system alters little the $-5/3$ spectra at shorter wavelength, but substantially the amplitude and the shape for the -3 spectra at longer wavelength. It has been demonstrated that the convectively intensified amplitudes at longer wavelengths result simply from the intermittent development of the MCS across the domain, rather than the upscale KE propagation. It should be noted, though, that this conclusion is only obtained from a single numerical case study in which numerous approximations are made. Some more carefully arranged numerical simulations should be conducted in the future, *e.g.*, with higher resolution, a larger domain and explicit convection, to provide a better understanding of the spectral characteristics of moist convection. Nevertheless, because this simulation has been extensively verified against all special network observations and because there are so many similarities between the observed and simulated squall systems, we believe that the basic conclusions presented herein are still relevant to real squall systems in midlatitudes, particularly for those trailed by extensive stratiform precipitation.

Acknowledgments

We wish to thank Profs. T. Warn and I. Zawadzki for their helpful discussions on the subject of kinetic energy spectra. The original model integration was performed on CRAY X-MP of the National Centre for Atmospheric Research, which is sponsored by the National Science Foundation. The research was partly supported by the Natural Science and Engineering Research Council and Atmospheric Environment Service of Canada.

References

Anthes, R.A., E.-Y. Hsie and Y.-H. Kuo, 1987: Description of the Penn State/NCAR mesoscale model version 4 (MM4). NCAR Tech. Note, NCAR/TN-282, 66 pp.

Augustine, J.A. and E.J. Zipser, 1987: The use of wind profiles in a mesoscale experiment. *Bull. Amer. Meteor. Soc.*, **68**, 4–17.

Biggerstaff, M.I. and R.A. Houze, Jr., 1991: Midlevel vorticity structure of the 10–11 June 1985 squall line. *Mon. Wea. Rev.*, **119**, 3066–3079.

Carney, T.Q. and D.G. Vincent, 1986: Meso-synoptic scale interaction during AVE/SESAME I, 10–11 April 1979. Part II: Influence of convective activity on larger scale flow. *Mon. Wea. Rev.*, **114**, 353–370.

Charney, J.G., 1971: Geostrophic turbulence. *J. Atmos. Sci.*, **28**, 1087–1095.

Chen, T.-C. and A. Wiin-Nielson, 1978: Nonlinear cascades of atmospheric energy and enstrophy. *Tellus*, **30**, 313–322.

Chen, S.-J., L.-S. Bai and E.C. Kung, 1990: An approach to kinetic energy diagnosis of meso-synoptic scale interactions. *Mon. Wea. Rev.*, **118**, 2774–2780.

Errico, R.A., 1985: Spectra computed from a limited area grid. *Mon. Wea. Rev.*, **113**, 1554–1562.

Fritsch, J.M. and C.F. Chappell, 1980: Numerical prediction of convectively driven mesoscale pressure systems. Part I: Convective parameterization. *J. Atmos. Sci.*, **37**, 1722–1733.

Fritsch, J.M. and R.A. Maddox, 1981: Convectively driven mesoscale weather systems aloft. Part I: Observations. *J. Appl. Meteor.*, **20**, 9–19.

Fritsch, J.M. and J.M. Brown, 1982: On the generation of convectively driven mesohighs aloft. *Mon. Wea. Rev.*, **110**, 1554–1563.

Fuelberg, H.E. and G.J. Jedlovec, 1982: A subsynoptic-scale kinetic energy analysis of the Red River Valley tornado outbreak (AVE-SESAME I). *Mon. Wea. Rev.*, **110**, 2005–2024.

Fuelberg, H.E. and M.F. Printy, 1984: A kinetic energy analysis of the meso-β-scale severe storm environment. *J. Atmos. Sci.*, **41**, 3212–3226.

Gage, K.S., 1979: Evidence for $k^{-5/3}$ law inertial range in mesoscale two-dimensional turbulence. *J. Atmos. Sci.*, **36**, 1950–1954.

Gallus, W.A., Jr. and R.H. Johnson, 1992: The momentum budget of an intense midlatitude squall line. *J. Atmos. Sci.*, **49**, 422–450.

Gao, K., D.-L. Zhang, M.W. Moncrieff and H.-R. Cho, 1990: Mesoscale momentum budget in a midlatude squall line: A numerical case study. *Mon. Wea. Rev.*, **118**, 1011–1028.

Houze, R.A., Jr., 1977: Structure and dynamics of a tropical squall-line system. *Mon. Wea. Rev.*, **105**, 1540–1567.

Houze, R.A., Jr., 1989: Observed structure of mesoscale convective systems and implications for large-scale heating. *Quart. J. Roy. Meteor. Soc.*, **115**, 425–461.

Houze, R.A., Jr., S.A. Rutledge, M.I. Biggerstaff and B.F. Smull, 1989: Interpretation of Doppler weather-radar displays of midlatitude mesoscale convective systems. *Bull. Amer. Meteor. Soc.*, **70**, 608–619.

Hsie, E.-Y., R.A. Anthes and D. Keyser, 1984: Numerical simulation of frontogenesis in a moist atmosphere. *J. Atmos. Sci.*, **41**, 2581–2594.

Johnson, R.H. and P.J. Hamilton, 1988: The relationship of surface pressure features to the precipitation

and airflow structure of an intense midlatitude squall line. *Mon. Wea. Rev.*, **116**, 1444–1472.

Johnson, R.H. and D.L. Bartels, 1992: Circulations associated with a mature-to-decaying midlatitude mesoscale convective system. Part II: Upper-level features. *Mon. Wea. Rev.*, **120**, 1301–1320.

Kolmogorov, A.N., 1941: The local structure of turbulence in incompressible viscous fluids for very large Reynolds numbers. *C.R. Acad. Sci. URSS*, **30**, 301–305.

Kung, E.C. and T.L. Tsui, 1975: Subsynoptic-scale kinetic energy balance in the storm area. *J. Atmos. Sci.*, **32**, 729–740.

Lilly, D.K., 1983: Stratified turbulence and the mesoscale variability of the atmosphere. *J. Atmos. Sci.*, **40**, 749–761.

Lilly, D.K. and B.F. Jewett, 1990: Momentum and kinetic energy budgets of a simulated supercell thunderstorms. *J. Atmos. Sci.*, **47**, 707–726.

Lin, Y.-J. and J.A. Coover, 1988: A kinetic energy analysis of a microburst-producing thunderstorm based on JAWS Dual-Doppler data. *J. Atmos. Sci.*, **45**, 2764–2771.

Lin, Y.-J., H. Shen and R.W. Pasken, 1991: Kinetic energy budgets of a subtropical squall line determined from TAMEX dual-Doppler measurements. *Mon. Wea. Rev.*, **119**, 2654–2663.

Maddox, R.A., 1983: Large-scale meteorological conditions associated with midlatitude mesoscale convective complexes. *Mon. Wea. Rev.*, **111**, 1475–1493.

Maddox, R.A., D.J. Perkey and J.M. Fritsch, 1981: Evolution of upper tropospheric features during the development of a mesoscale convective complex. *J. Atm. Sci.*, **38**, 1664–1674.

McInnis, D.H. and E.C. Kung, 1972: A study of subsynoptic scale energy transformations. *Mon. Wea. Rev.*, **100**, 126–132.

Nastrom, G.D. and K.S. Gage, 1984: A climatology of atmospheric wavenumber spectra of wind and temperature observed by commercial aircraft. *J. Atmos. Sci.*, **42**, 950–960.

Rotunno, R., J.B. Klemp and M.L. Weisman, 1988: A theory for strong, long-lived squall lines. *J. Atmos. Sci.*, **45**, 463–485.

Rutledge, S.A. and R.A. Houze, Jr., 1987: A diagnostic modeling study of the trailing stratiform region of a midlatitude squall line. *J. Atmos. Sci.*, **44**, 2640–2656.

Rutledge, S.A., R.A. Houze, Jr., M.I. Biggerstaff and T. Matejka, 1988: The Oklahoma-Kansas mesoscale convective system of 10–11 June,1985: Precipitation structure and Single-Doppler radar analysis. *Mon. Wea. Rev.*, **118**, 1011–1028.

Smull, B.F. and R.A. Houze, Jr., 1987: Rear inflow in squall lines with trailing stratiform precipitation. *Mon. Wea. Rev.*, **115**, 2869–2889.

Srivastava, R.C., 1985: A simple model of evaporatively driven downdraft: Application to microburst downdraft. *J. Atmos. Sci.*, **42**, 1004–1023.

Tsui, T.L. and E.C. Kung, 1977: Subsynoptic-scale energy transformations in various severe storm situations. *J. Atmos. Sci.*, **34**, 98–110.

Uccellini, L.W. and D.R. Johnson, 1979: The coupling of upper and lower tropospheric jet streaks and implications for the development of severe convective storms. *Mon. Wea. Rev.*, **107**, 682–703.

Vincent, D.G. and T.W. Schlatter, 1979: Evidence of convection as a source of synoptic-scale kinetic energy. *Tellus*, **31**, 493–504.

Vincent, D.G. and T.Q. Carney, 1984: Differences between KE budget terms derived from SESAME and NWS data sets. *Mon. Wea. Rev.*, **112**, 2347–2353.

Zhang, D.-L., 1989: The effect of parameterized ice microphysics on the simulation of vortex circulation with a mesoscale hydrostatic model. *Tellus*, **41A**, 132–147.

Zhang, D.-L., 1992: The formation of a cooling-induced mesovortex in the trailing stratiform region of a midlatitude squall line. *Mon. Wea. Rev.*, **120**, 2763–2785.

Zhang, D.-L. and R.A. Anthes, 1982: A high-resolution model of the planetary boundary layer—sensitivity tests and comparisons with SESAME-79 data. *J. Appl. Meteor.*, **21**, 1594–1609.

Zhang, D.-L., H.-R. Chang, N.L. Seaman, T.T. Warner and J.M. Fritsch, 1986: A two-way interactive nesting procedure with variable terrain resolution. *Mon. Wea. Rev.*, **114**, 1330–1339.

Zhang, D.-L. and J.M. Fritsch, 1988: Numerical sensitivity experiments of varying model physics on the structure, evolution and dynamics of two mesoscale convective systems. *J. Atmos. Sci.*, **45**, 261–293.

Zhang, D.-L., K. Gao and D.B. Parsons, 1989: Numerical simulation of an intense squall line during 10–11 June 1985 PRE-STORM. Part I: Model verification. *Mon. Wea. Rev.*, **117**, 960–994.

Zhang, D.-L. and K. Gao, 1989: Numerical simulation of an intense squall line during 10–11 June 1985 PRE-STORM. Part II: Rear inflow, surface pressure perturbations and stratiform precipitation. *Mon. Wea. Rev.*, **117**, 2069–2094.

Zhang, D.-L. and H.-R. Cho, 1992: The development of negative moist potential vorticity in the stratiform region of a simulated squall line. *Mon. Wea. Rev.*, **120**, 1322–1341.

中緯度スコール系のメソβスケールの運動エネルギー解析

張　大林・王　志明
(マギル大学・大気海洋科学学部)

中緯度に発現したメソスケール対流系 (MCS) のメソβスケールの運動エネルギー (KE) と大規模場の流れへの影響を調べた。このために、1985 年 6 月 10–11 日に PRE-STORM で観測されたスコール系について、実際のデータをもとに高解像の数値モデルを 21 時間時間積分した。スコール系の KE は、主に front-to-rear (FTR) の上昇流域の圧力項によって生成され、また主に水平フラックス発散によって失われた。鉛直フラックス発散は、上層ジェットの下 (上) の FTR の上昇流域では KE を減らした (増やした)。それに対して、rear-to-front (RTF) の下降流域では鉛直フラックス発散はいつも KE を増加させた。RTF の下降流域での KE の下流への輸送によって、スコールラインに平行にある大きな KE を持つジェットストリームは、スコール系や地表のガストフロントの強さに影響を及ぼしたようである。

解像されるあらゆるスケールの大気運動への湿潤対流の効果を波数空間で調べた。深い対流を入れることによって、短波長域では KE スペクトルはあまり変わらなかったが、長波長域ではスペクトルの強さとスロープが大きく変化した。この変化は、KE の逆カスケードによるというよりも MCS の間欠的な発達のためと思われる。